

Bifurcations of the thermohaline circulation in a simplified three-dimensional model of the world ocean and the effects of interbasin connectivity.

Neil R. Edwards¹ and John G. Shepherd²

1. *L.E.G.I. Grenoble, France*

2. *Southampton Oceanography Centre, U.K.*

September 17, 2001

Abstract

A coarse-resolution, global, three-dimensional, idealised model of the world ocean, based on the thermocline equations, is described. It is demonstrated that, at suitable resolution, such a model can be integrated for 100's or 1000's of millenia, and could therefore form a component of an earth system model designed to investigate climate change on these timescales. As in other ocean models, the thermohaline circulation is found to exhibit multiple stable states. The bifurcation structure of the model has been explored, as a function of surface saline forcing, and is found to depend on the inter-basin connectivity, the topography, and the form of the imposed wind forcing.

1 Introduction

Previous work with simplified, two-dimensional models of the oceanic thermohaline circulation (Marotzke et al. 1988, Stocker and Wright 1991, Wright and Stocker 1991, Thual and McWilliams 1992, Dijkstra and Neelin 2000) has shown

(a) that they are capable of producing plausible magnitudes and structures for the oceanic thermohaline circulation, at least when representing the Atlantic Ocean, where an equatorially asymmetric northern sinking mode obtains in the real world, despite approximately symmetric forcing of both heat and salt fluxes,

(b) that multiple stable states appear to exist, and that sharp transitions between them are possible when the magnitude of salt flux forcing is varied.

Some of the same features have been found in 3-D models (Bryan 1986, Manabe and Stouffer 1988, Marotzke and Willebrand 1991, Rahmstorf 1994,

1995, Marotzke and Klinger 2000). However, recent advances in understanding the physical controls on the thermohaline circulation (THC) (Marotzke and Klinger 2000) suggest that it is possible that 2-D models which must parameterize the effects of the Earth’s rotation may arrive at plausible representations of the THC for the wrong physical reasons, or at least may be quantitatively unreliable. The magnitude of this problem is not yet clear. This could mean that projections with such models under substantially different forcing regimes, such as may obtain for palaeoclimate and greenhouse warming simulations, may be unreliable. Since the heat and freshwater transports by the oceans are first-order contributions to the global fluxes, this could have serious consequences for climates so modelled. However, 2-D models have many advantages, especially simplicity and computational efficiency, which enable extensive sensitivity testing of model simulations, as well as the potential for producing adequate ensembles of runs where stochastic forcing or dynamics are introduced.

Our interest in simplified ocean models stems from the need to represent the oceans as efficiently and faithfully as possible in integrated earth system models of intermediate complexity (EMIC’s). Considering the possible drawbacks of 2-D models mentioned above, we have been motivated to explore, in the present work, the efficiency and physical behaviour of an extremely coarse 3-D ocean model. Simplified physics are used based on the so-called thermocline equations appropriate for long-term and large-scale motions. The major ocean basins are represented in the coarsest reasonable way and the equations are solved using minimal resolution in the zonal direction. The model thus lies somewhere in between an ensemble of box models and a well-resolved thermocline model. We thus refer to the model informally as a “lego-box” global model.

Our principal aims are two-fold: firstly to determine whether such a model can yet be run sufficiently fast on available hardware to be suitable as the ocean component of an EMIC intended for studies on timescales up to and including the major glacial-interglacial cycles $O(100\text{ka})$ and if so, at what spatial resolution; secondly to determine whether multiple stable states occur in such a model, and if so to determine the broad features of such states.

2 The model

The model is based on the thermocline (or planetary geostrophic) equations, with the addition of a linear drag term in the horizontal momentum equations. In the resulting “frictional geostrophic” system, density depends nonlinearly on the local values of temperature T and salinity S , which obey separate advection-diffusion equations and are also subject to convective adjustment. Apart from the treatment of islands, described in the Appendix, and the inclusion of velocity relaxation, as described by Edwards and Shepherd (2001) (henceforth referred to as ES), the model is essentially as used by Edwards et

al. (1998) (henceforth EWK), and is described more fully therein.

A condition of no normal flow is applied at all boundaries. At the lateral boundaries we also specify zero normal fluxes of heat and salt. At higher resolution it is desirable to use the more complicated integral boundary condition of Samelson and Vallis (1997) to avoid numerical restriction of the timestep, see ES, but the resolution of our model makes such a condition inappropriate. The lower boundary fluxes of T and S are set to zero while at the upper boundary mixed boundary conditions are used to give the required thermohaline forcing. Thus the flux of temperature out of the top grid box is given by

$$F_T = -\frac{T_a - T}{\tau_r} \Delta z, \quad (1)$$

where Δz is the depth of the top grid cell, T is the temperature in the top grid cell, τ_r is a restoring timescale, and the prescribed apparent atmospheric temperature T_a is a cosine function of latitude θ given by

$$T_a = A \cos\left(\frac{\pi\theta}{2\theta_1}\right), \quad (2)$$

where the domain has been assumed to extend from $-\theta_1$ to θ_1 . The (upward) surface salinity flux per unit area is defined as the gradient of a northward salinity transport, and is given by

$$F_S = -\frac{D}{2\pi} \frac{\partial}{\partial s} \left(\sin\left(\frac{\pi\theta}{\theta_1}\right) \right) - C, \quad (3)$$

where $s = \sin\theta$, the constant C is chosen such that the globally integrated surface salinity flux is zero, and the constant D , representing the magnitude of the zonally integrated northward salinity transport, determines the strength of the saline forcing. If a wind stress is imposed, it is assumed to decrease linearly to zero over the uppermost grid cell.

The default values of the model parameters are given in Table 1. Note that the values used for horizontal and vertical diffusivities, κ_h and κ_v and momentum drag (Rayleigh friction) coefficient λ must be large at this low resolution to maintain stability and to represent a wide range of unresolved transport processes. The surface salinity flux amplitude D equates to 0.212 m/year fresh water flux.

The model domain is shown schematically in Figure 1. It consists of 3 rectangular basins representing the Pacific, Atlantic and Indian oceans, connected at the south by a periodic channel representing the Southern Ocean. For the lowest resolution implementation used as standard, the model Pacific is 6 cells wide and the model Atlantic and Indian Oceans are 3 cells wide. The model Pacific and Atlantic Oceans are connected by a strait one cell wide representing Drake Passage. The domain extends from 70°S to 70°N and the grid spacing is uniform in longitude ϕ and $\sin(\text{latitude})$ s . Thus the northern boundary of the model Pacific lies at 47.0°N ; the northern boundary of

Table 1: Default parameter values.

parameter	value
A	25 ⁰ C
θ_1	70 ⁰
D	6×10^7 psu m ³ s ⁻¹
λ	(0.625 days) ⁻¹
κ_h	12000 m ² s ⁻¹
κ_v	2×10^{-4} m ² s ⁻¹
τ_r	61 days

the model Indian Ocean is at 18.3⁰N; the southern boundaries of the model landmasses representing Africa and Australasia are at 38.8⁰S and the model Drake passage lies between 56.6⁰S and 70⁰S. The longitudinal grid spacing is 20⁰, thus the width of the model Pacific is 120⁰ and the model Atlantic and Indian Oceans are both 60⁰ wide. We will also discuss solutions in the same domain in which the horizontal grid resolution is increased by a factor of either 2 or 4. In the vertical there are 8 density levels on a logarithmically stretched grid with vertical spacing increasing with depth from 140 m to 1120 m. The maximum depth is set to 4 km.

For the 18×18 grid used for most of our experiments we use a time step of 2 weeks. The computational efficiency of the model will be demonstrated in Section 4 where we exhibit the results of sequences of runs, each corresponding to a total integration time of a million years.

3 Steady solutions

The model is initialised with a state of uniform salinity. The initial temperature is also uniform in each hemisphere, but we allow for a difference between the initial values T^- and T^+ in the southern and northern hemispheres to favour possibly different asymmetric steady solutions, although this is shown later to have very little effect. We return to the question of multiple solutions later. For the solutions discussed below T^- and T^+ have, unless stated otherwise, been set to 25 and 20 degrees respectively. The model is integrated forwards in time until the solution reaches a quasi-steady state, the form of which depends on the relative strength of the salinity forcing $R = D/D_0$ where D_0 is the standard value given in Table 1 (thus $R = 1$ corresponds to a salinity forcing amplitude of about 0.2 m/year fresh water).

An example solution is presented in Figure 2, which shows vertical-meridional sections of temperature and velocity at mid-basin in the model Pacific and Atlantic, in computational space, at about 1000 years, with $R = 0.1$. By this time the solution is essentially steady. Cold water is produced by the surface forcing in the Southern Ocean and in the north Atlantic and sinks to the bottom, the

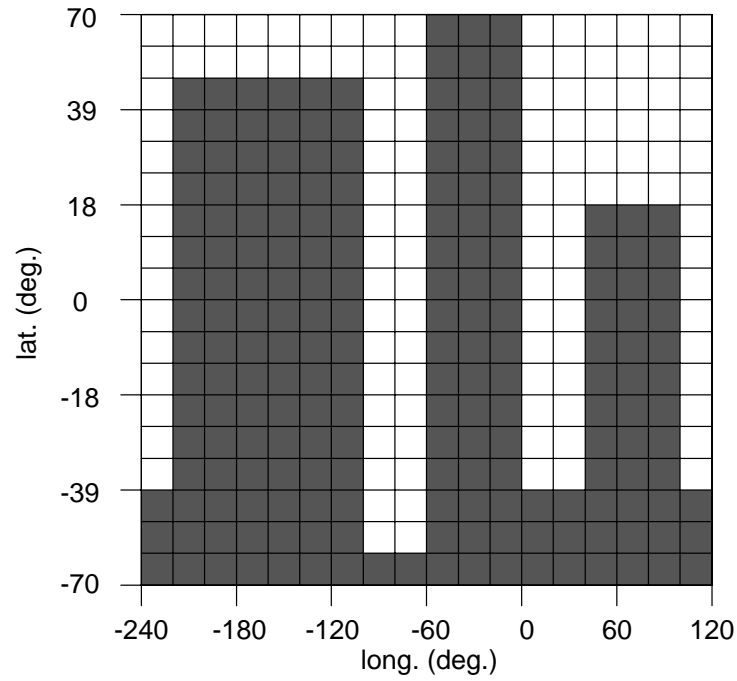


Figure 1: Diagram of the model domain with ocean cells shaded dark grey showing, from left to right, the model Pacific, Atlantic and Indian oceans.

Atlantic being a degree or two colder than the Pacific below the surface layers. In the Atlantic a roughly symmetric two-cell overturning circulation results (the meridional overturning streamfunctions are plotted below in Figure 3). The northern boundary of the Pacific is at a lower latitude than its southern boundary and the north Pacific surface water is consequently less dense, sinking only to intermediate depth and allowing the southern sinking cell to dominate the Pacific basin. Convection occurs all along the southern boundary of the domain, reaching the bottom in the southwest Pacific, in Drake Passage and in between the Atlantic and Indian oceans. Deep convection, to the second model level from the bottom, also occurs in the northwest Atlantic, while only shallow convection occurs in the north Pacific. The north Indian has no convecting points. The salinity field has a similar spatial structure to the temperature field, except that the fixed-flux forcing results in generally higher surface salinities in the Pacific and Indian, as compared to the Atlantic. The strongest velocities occur in western boundary currents, whose directions reverse at mid-depths, and in the Southern Ocean, particularly close to Drake Passage. There is no barotropic flow in this run, and the Southern Ocean flow is generally eastwards in the upper layers and westwards at depth. Note that we have made no attempt to “tune” the results of the model (such as the bottom water temperatures or the Atlantic-Pacific salinity difference) to current observations, since our interest here is restricted to the qualitative behaviour of the model under a wide range of forcing conditions.

At this resolution, horizontal gyre circulations must be viewed as being “represented”, rather than resolved, much in the way that the meridional overturning cells of the thermohaline circulation are “represented” by box models (the effect of wind-driven gyres is considered in Section 4.5). Our standard resolution thus represents an interesting hybrid between box models and resolved models, and is close to the minimum resolution for a 3-D global domain with a representation of ocean basin geometry. In ES it was shown that the present model has reasonable behaviour, in a simple basin, at a range of resolutions from a $2 \times 2 \times 2$ box model to a $16 \times 16 \times 16$ version.

Figure 3 shows the meridional overturning streamfunctions, defined to the north of the Southern Ocean, for the model Atlantic and Pacific, for 4 runs at various values of R . As discussed by Thual and McWilliams (1992) and Dijkstra and Neelin (2000), increasing the magnitude of saline forcing destabilizes the polar-sinking, 2-cell mode in the Atlantic, so that for large enough R the solution converges towards a predominantly single-cell Atlantic state. In the sequence of runs shown in Figure 3, the northern-sinking (positive) Atlantic cell weakens between $R = 0.1$ (b), and $R = 1$, (d), but then strengthens and ultimately becomes dominant for $R = 1.5$, (f). The model Pacific has only weak northern sinking for $R = 0.1$, (a), but Pacific northern sinking increases as R increases and becomes the dominant mode for $R = 2$. The maximum overturning in the Atlantic is 18 Sv at $R = 0.1$, 11 Sv at $R = 1$, 30 Sv at $R = 1.5$ and 38 Sv at $R = 2.0$.

The effect of these changes in circulation on the northward heat flux in the

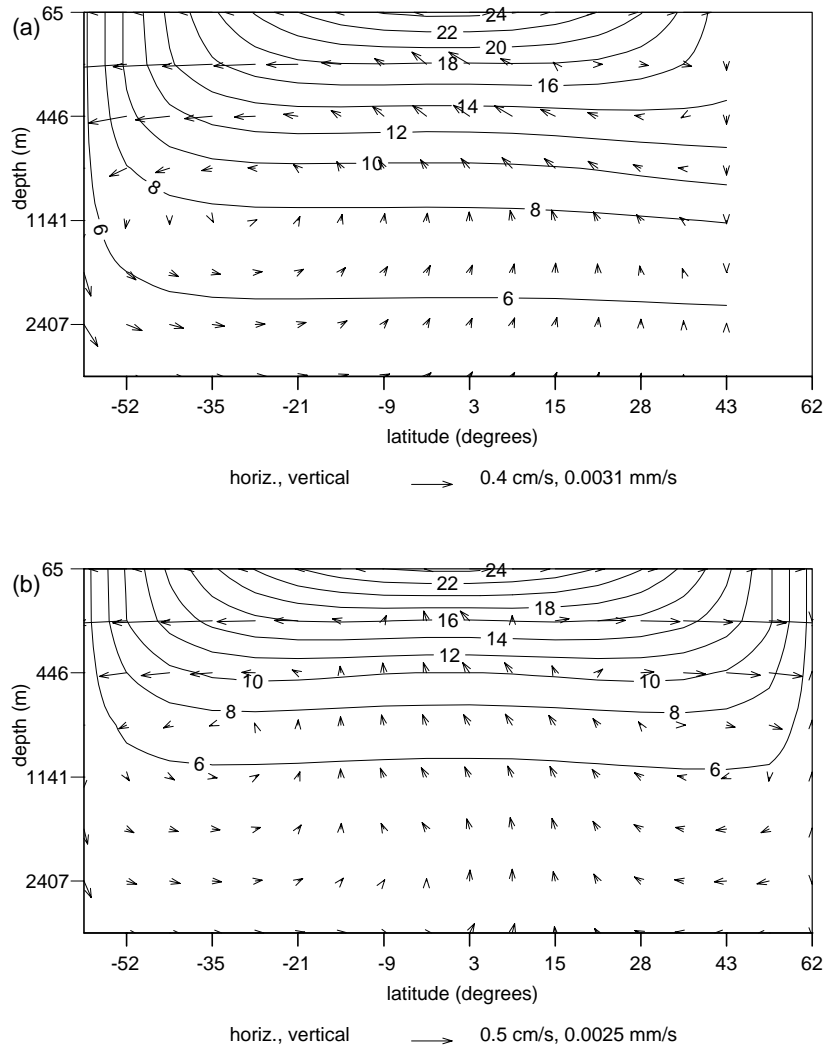


Figure 2: Meridional-vertical sections of temperature and velocity in the mid-Pacific (a) and mid-Atlantic (b), in model grid coordinates, for a steady state with weak saline forcing $R = 0.1$.

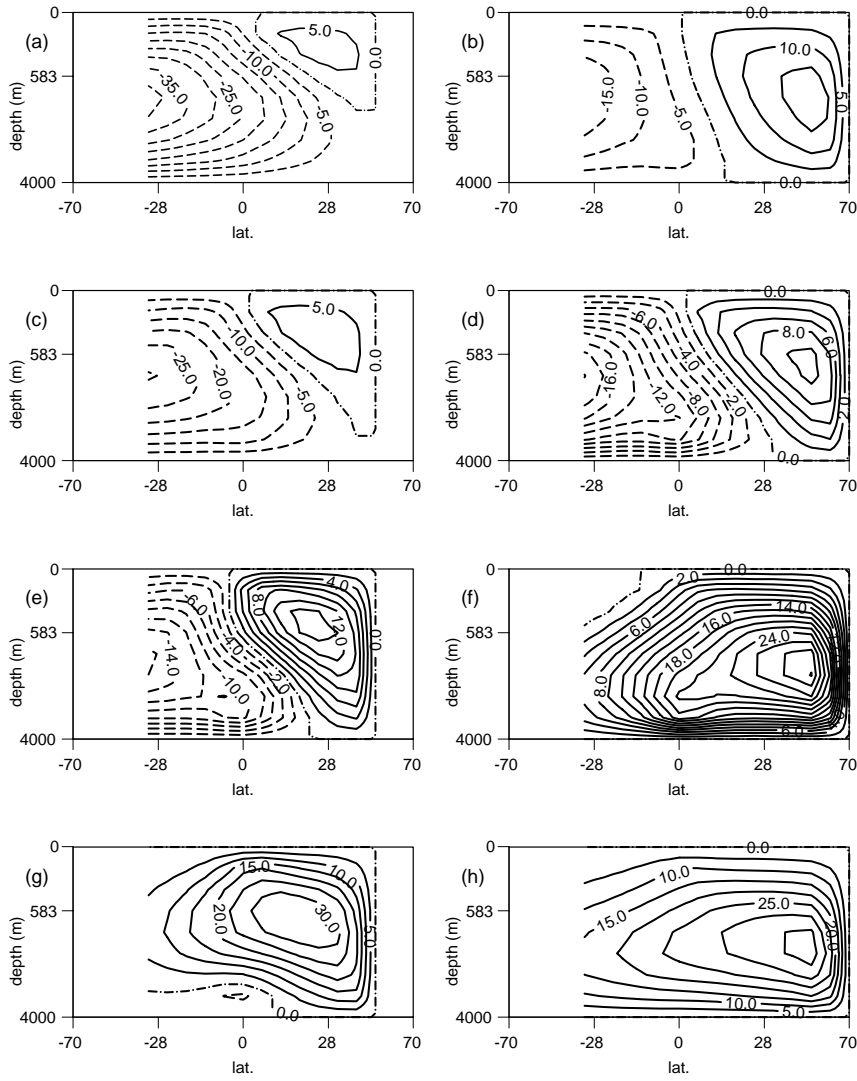


Figure 3: Meridional overturning streamfunctions in Sv, defined to the north of the Southern Ocean, for 4 runs at different values of relative salinity forcing amplitude R : (a) Pacific and (b) Atlantic at $R = 0.1$; (c) Pacific and (d) Atlantic at $R = 1$; (e) Pacific and (f) Atlantic at $R = 1.5$; (g) Pacific and (h) Atlantic at $R = 2$.

model is illustrated in Figure 4, in which the total global northward heat flux in the model is shown, together with the contributions of the model Pacific and Atlantic. The Pacific and Atlantic contributions are further decomposed into their advective and diffusive components. With the parameters of our coarse resolution model the diffusive components represent a wider range of processes than at higher resolution and are comparable in magnitude to the advective components. All these zonally integrated fluxes are shown as functions of latitude for $R = 1, 1.5$ and 2 . At $R = 1$, Figure 4(a), the dominance of the southern-sinking cells in both Atlantic and Pacific results in strong southward flux, peaking at -3.8 PW, and a much weaker northward maximum of only 1.1 PW. Figure 4(b) shows that the diffusive flux in the Pacific is mostly southward, as a result of the strong meridional temperature gradients in the south Pacific. In the Atlantic, Figure 4(c), the diffusive fluxes are comparable to the advective fluxes in both hemispheres, but note that the large thermal gradients imply large density gradients and hence unrealistic diapycnal diffusion—a drawback of the simplicity of this model. At $R = 1.5$ the switch to an essentially northern-sinking Atlantic results in a mostly northward Atlantic heat flux in Figure 4(d). The global heat flux curve is now more symmetrical with extrema of -2.7 and $+1.8$ PW. At $R = 2$ the Pacific circulation is also dominantly northern-sinking and the global flux, Figure 4(g), is stronger in the northward branch, the extrema being -1.5 and $+2.5$ PW. Pacific and Atlantic advective fluxes are both entirely northward at this value of R , but a significant southward diffusive heat flux remains in the Pacific, which is almost matched by the residual southward contribution to the global flux. This residual, mostly due to the Indian Ocean, has a similar magnitude for all three values of R .

We have carried out a limited investigation of the effect of increasing the horizontal resolution by repeating some of the above runs, retaining the identical domain and forcing functions. In Figure 5 we plot the total northward heat flux together with the Pacific and Atlantic contributions for two such runs at 2 and 4 times the standard resolution with salinity forcing $R = 2$ at about 2000 years (starting from a uniform initial temperature) by which time the solutions have become steady. These graphs should be compared with those from the corresponding run at lower resolution plotted in Figure 4(g). The graphs are qualitatively the same, suggesting that the basic model is capable of capturing the essential features of the meridional circulation in spite of the extremely coarse resolution, particularly in the zonal direction. Quantitatively, the maximum northward heat flux in the basic model on an 18×18 grid at 2000 years for $R = 2$ is 2.59 PW. On a 36×36 grid the corresponding value is 2.76 and on a 72×72 grid the value is 2.77 . Thus increased resolution in this case changes this particular global diagnostic parameter by less than 10%.

Previous studies of the thermohaline circulation in a single basin (see Introduction) have found that multiple, stable, steady states can exist for a range of values of saline forcing. The same is true in our model. For saline forcing strength $R = 1$ and $R = 1.5$, for instance, we can obtain steady solutions

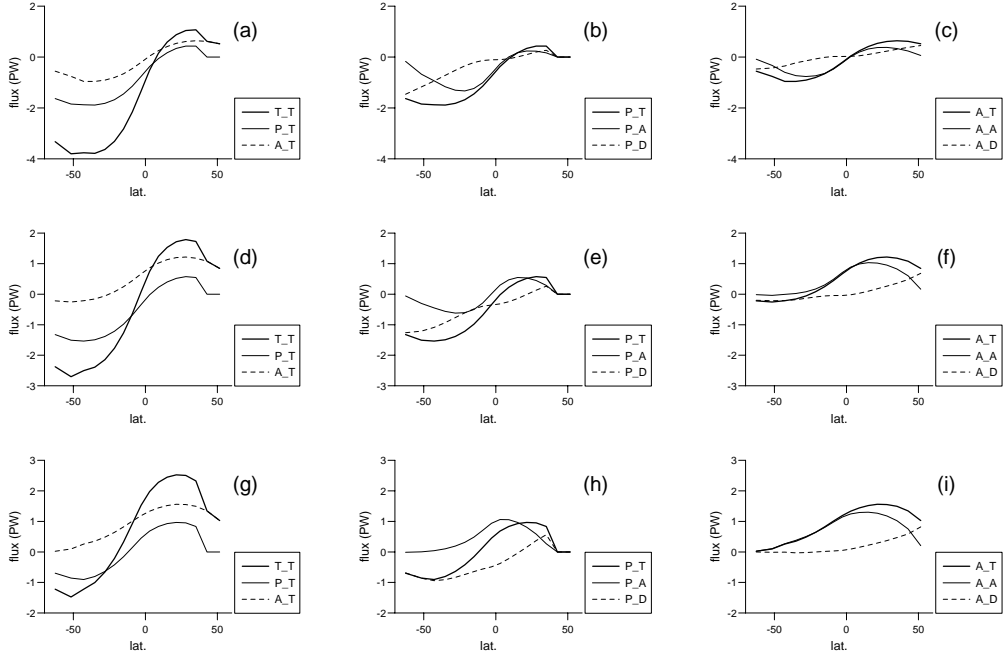


Figure 4: Integrated northward heat flux at various values of relative salinity forcing amplitude R and its advective and diffusive components. (a) Global, G_T ; Pacific, P_T and Atlantic, A_T fluxes at $R = 1$; (b) total northward flux in the Pacific, P_T and its advective, P_A and diffusive, P_D components at $R = 1$; (c) as (b) for the Atlantic; (d), (e) and (f) as above for $R = 1.5$; (g), (h) and (i) as above for $R = 2$.

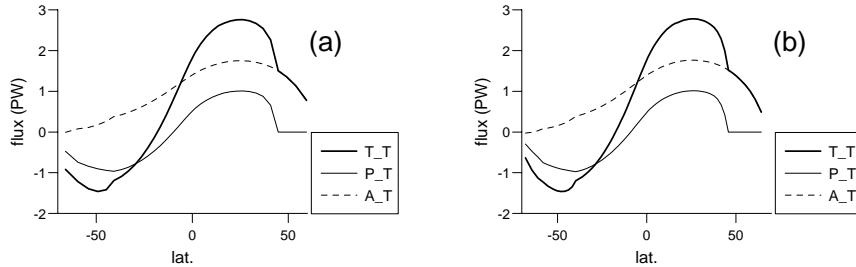


Figure 5: Globally integrated northward heat flux (thick line) with Pacific (thin) and Atlantic (dashed) components at $R = 2$ with (a) 2 times and (b) 4 times the standard resolution used above (compare with Figure 4(g)).

which are substantially different from those described above by integrating the model from a different initial state. Differences of a few degrees between the initial temperatures in the north T^+ and in the south T^- turn out to have no significant effect, but by starting from a cold initial state with $T \equiv 0$ instead of the warm initial state used above, we find a solution for $R = 1$ with the strength of the northern sinking north Atlantic cell roughly twice that of the southern cell. This is roughly the reverse situation to the solution shown above in Figure 3(d) for the same value of R . The Pacific circulation, by contrast, is very similar, thus this solution has strong sinking in the north Atlantic but not the north Pacific, in common with the present observed situation in the real ocean. For $R = 1.5$ starting from a cold initial state, $T \equiv 0$, produces a solution with a single dominant cell in the Pacific similar to that shown above for $R = 2$ in Figure 3(g) and (h). In the next section we consider more systematically the bifurcation between different flow regimes as R varies in the model.

4 Bifurcation sequences

In order to understand better how the thermohaline circulation in the model depends on the strength of the saline forcing and the initial conditions, as well as the multiple-basin geometry, we now consider a sequence of many model runs, each of which has constant salinity forcing parameter R , where we vary R in small increments between the individual runs and initialise each with the final state of the previous run. By first increasing and then decreasing R in this way we can search systematically for the presence of hysteresis and multiple solutions. Figure 6 shows the maximum (positive) and minimum (negative) values of the meridional overturning streamfunctions in the Pacific

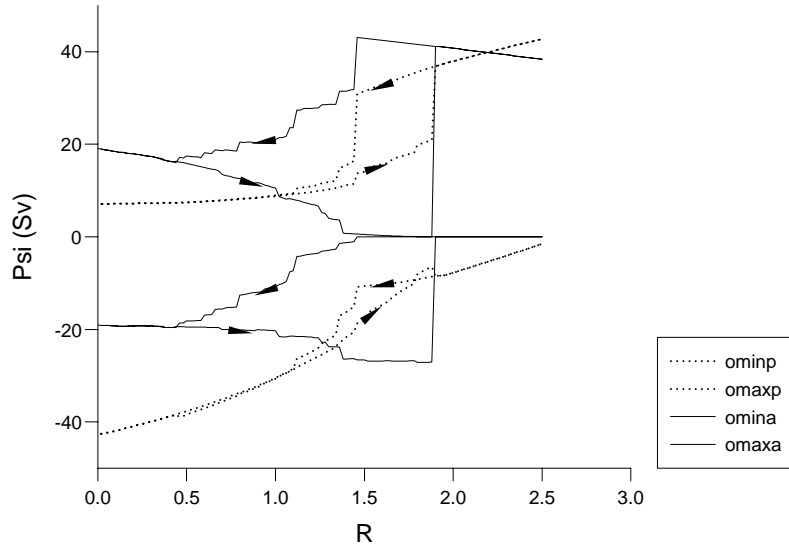


Figure 6: Maximum (positive) and minimum (negative) value of meridional overturning in the Atlantic, continuous line; and Pacific, dotted, for a sequence of runs with increasing and then decreasing relative salinity forcing amplitude R in the fully connected model, case C.

and Atlantic for such a sequence of runs. In this and the subsequent bifurcation sequences to be described, the incremental change in R between runs was 0.02 and the length of each run was 4000 years. For small R the Atlantic circulation is roughly symmetrical and the maximum and minimum values of overturning have roughly equal magnitude. As R is increased the increased salinity forcing leads to a reduction in the maximum Atlantic overturning but the minimum increases slightly in magnitude. As R is increased beyond about 1.4 the Atlantic circulation is dominated by the negative, southern-sinking cell until the flow switches to the reverse state with a single, northern-sinking cell for $R > 1.9$. The Atlantic circulation shows considerable hysteresis, since the circulation remains in a single cell, northern-sinking state, when R is decreased, until about $R = 1.4$, and northern sinking remains the dominant mode until $R = 0.6$. The region of multiple Atlantic states extends from $R = 0.44$ to $R = 1.9$. Major bifurcations in the Atlantic circulation are

accompanied by bifurcations in the Pacific circulation, which has a smaller region of significant hysteresis for $1.4 < R < 1.9$. The dominant negative cell in the Pacific weakens monotonically as R increases from zero while the positive, northern-sinking cell strengthens, also monotonically. The Pacific extrema also change monotonically on the return branch as R decreases, but the northern sinking state persists to smaller values of R , as in the Atlantic.

This sequence of runs puts the solutions of the previous section into perspective. At $R = 1.5$ the system is close to a major bifurcation and the solution shown above is somewhat intermediate in character. Otherwise the solutions of the previous section obtained with a warm initial condition correspond closely to states on the increasing- R branch. Those mentioned at the end of the section obtained using cold initial conditions turn out to correspond to states on the decreasing- R branch.

It is instructive to compare the behaviour of the global model, thus obtained, with the behaviour of variants on the model geometry in which communication between the different basins is prevented. In the first such experiment, denoted A, we block the Southern, circumpolar ocean at Drake Passage and south of Africa, creating an isolated, rectangular Atlantic, with the Indian and Pacific remaining connected. In the second experiment, we block the Southern ocean at Drake Passage and also to the south of Australasia. In this experiment, denoted P, the model Pacific is an isolated, rectangular basin but the Atlantic and Indian oceans remain connected. In the third experiment, denoted D, only the Drake Passage is closed. In each case we use the same forcing functions as above except that the net salt flux into each isolated basin is set to zero by defining the constant C of Eq. (3) separately for each basin. Bifurcation diagrams for these experiments are shown in Figures 7, (case A), 8, (case P) and 9, (case D). The fully connected case will be referred to henceforth as case C.

4.1 Isolated Atlantic Case A

In case A, figure 7, the Atlantic system is isolated and symmetrical and shows a bifurcation sequence qualitatively as expected from the results of ES and Thual and McWilliams (1992). For small R the solution is symmetrical (note that the meridional overturning streamfunction for an isolated basin is only defined within the range of latitudes where the basin is bounded to east and west; we use the same defining latitude limits even when the basins are 'artificially' closed, for ease of comparison, thus the extremal overturning values may be underestimated if they occur close to the southern boundary). At larger R the solution switches to an essentially single-cell, northern-sinking state and there is a region of hysteresis where both 1-cell and 2-cell solutions are found. The switch to a northern rather than a southern-sinking state is determined by the small asymmetry in the initial condition for the first run. As R is increased, the sum of the absolute maxima of overturning steadily decreases, as a result of the competition between thermal and saline forcing. The Pacific, which

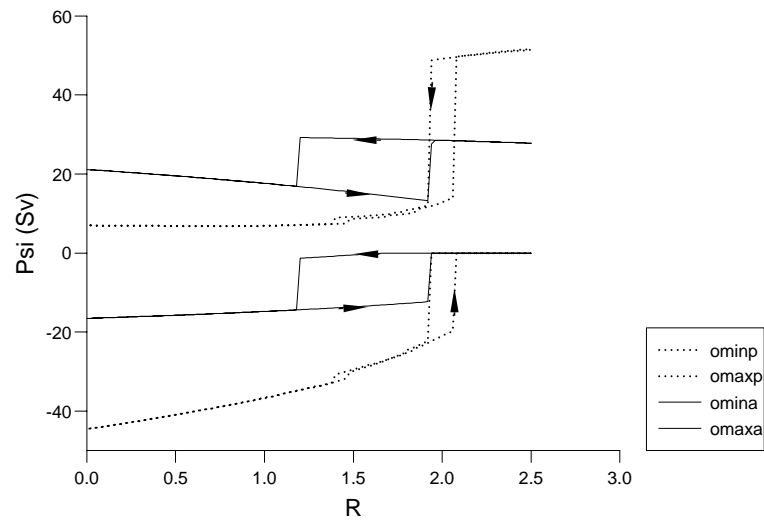


Figure 7: Maximum (positive) and minimum (negative) value of meridional overturning in the Atlantic, continuous line; and Pacific, dotted, for a sequence of runs with increasing and then decreasing relative salinity forcing amplitude R with the circumpolar ocean blocked at Drake Passage and to the south of Africa, isolating the Atlantic, case A.

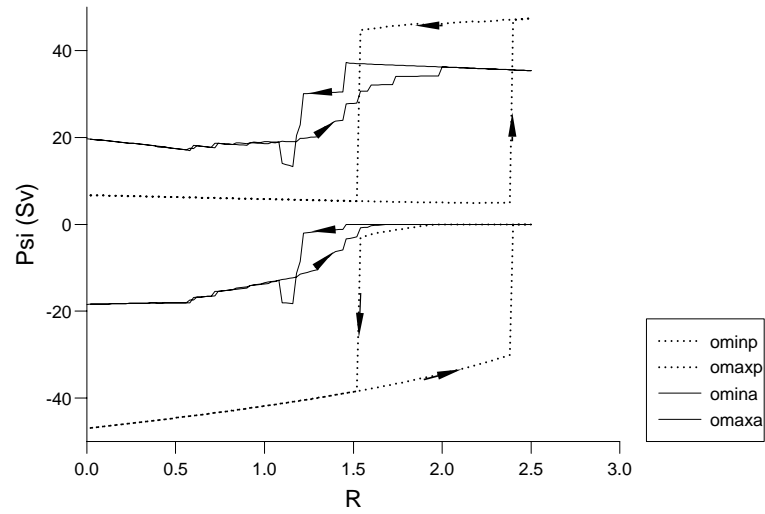


Figure 8: Maximum (positive) and minimum (negative) value of meridional overturning in the Atlantic, continuous line; and Pacific, dotted, for a sequence of runs with increasing and then decreasing relative salinity forcing amplitude R with the circumpolar ocean blocked at Drake Passage and to the south of Australasia, isolating the Pacific, case P.

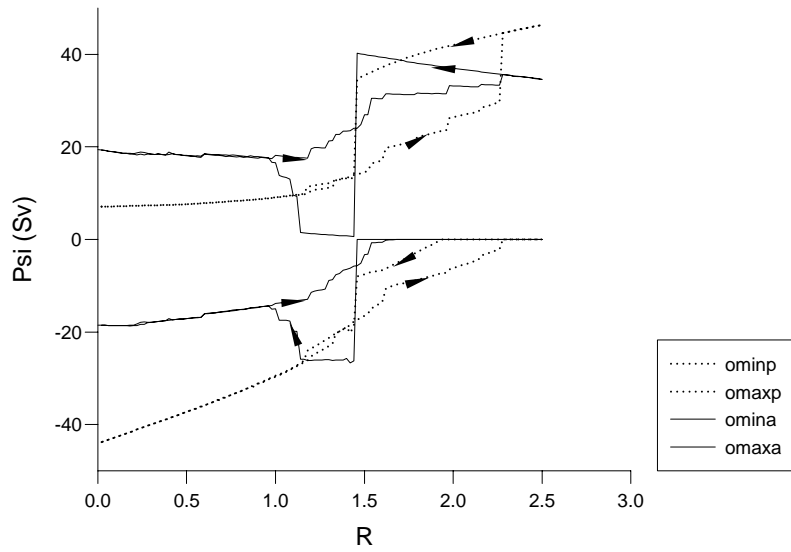


Figure 9: Maximum (positive) and minimum (negative) value of meridional overturning in the Atlantic, continuous line; and Pacific, dotted, for a sequence of runs with increasing and then decreasing relative salinity forcing amplitude R with the Drake Passage closed, case D.

is connected to the Indian and Southern oceans, shows similar behaviour, although small differences between the outward and return branches persist outside the main region of hysteresis. Note that there may be other steady solutions, since single runs at fixed R were not always found to converge to points on either branch of the bifurcation sequence. The coincidence of the bifurcation points at $R = 1.92$ is an accident of the choice of parameters and is removed by a 3% change in vertical diffusivity.

4.2 Isolated Pacific Case P

In case P, figure 8, we see that the Pacific behaves similarly to the Atlantic when isolated, although in the two-cell state at low R , the positive, northern cell is relatively weaker as a result of the asymmetry of the domain. Meanwhile, when connected to the Indian and Southern oceans, changes in the Atlantic overturning proceed in a series of steps. This may be partly due to the coarse resolution and the complex geometry, closer inspection shows that individual steps in the Atlantic overturning curve correspond to transitions between convecting and non-convecting states in particular grid cells. However, the results of Lenderink and Haarsma (1994) show that such non-smoothness can persist at higher spatial resolution as whole areas containing many grid cells can switch between convecting states.

4.3 Fully connected Case C revisited

In the fully connected case C, figure 6, both Pacific and Atlantic curves show stepwise evolution with R , reinforcing the conclusion that the geometry of the inter-basin connections contribute to this behaviour in our model. Both major basins bifurcate to northern-sinking, single-cell states at large R with the most dramatic increase in positive overturning occurring simultaneously for the two basins at $R = 2$. The most dramatic decrease in positive overturning on the return branch also occurs at the same point, $R = 1.5$ for both major basins, roughly half-way between the corresponding jumps for the two isolated ocean systems in case A.

Further indication of a form of averaged behaviour for the connected system is provided by the relatively similar values of maximal overturning in the Atlantic and Pacific at large R in the connected system, as compared to the isolated Atlantic case. In the connected case there is stronger overturning in the Atlantic and weaker overturning in the Pacific. The sums of the four absolute overturning maxima from the two basins at $R = 2.5$ are similar; 78 Sv in case C as against 79 in case A and 83 in case P. Similarly, for smaller R , note that the Pacific negative (southern sinking) cell weakens significantly as R is increased from 0 to 2.5 in case C, but is weakened less strongly when connected only to the Indian and southern oceans in case A, and even less strongly when fully isolated. Meanwhile the Atlantic negative cell, by contrast, becomes stronger as R increases from 0 to about 1.9 in the connected

case C, while in cases A and P, without the connection to the Pacific, the negative cell weakens over this range, although the sum of the two overturning extrema in the Atlantic is similar in all three cases. Thus it appears that the weakening of the Pacific negative, southern-sinking cell and the strengthening of the corresponding Atlantic cell seen in the fully connected case (Figure 6) rely on the connection between the two basins. The major Pacific negative cell is apparently weakened by the connection to the other basins.

4.4 Closed Drake Passage Case D

In case A (Figure 7), with the Atlantic isolated and the Pacific connected only to the Indian Ocean, the Pacific negative cell weakens as R increases, but less so than in the fully connected case. On the other hand closing only the Drake Passage has little effect on the Pacific negative cell which behaves roughly as in the fully connected case C (compare Figures 6 and 9). In other words the Pacific circulation is strongly affected by the remote connection to the Atlantic via the Indian Ocean, even with no depth-averaged Antarctic circumpolar current (ACC). The model Atlantic circulation, by contrast, is strongly affected by closing only Drake Passage. Although the Pacific negative cell weakens as R increases, the Atlantic negative cell appears unable to benefit from this and both Atlantic cells initially weaken, as in case A with the Atlantic completely isolated. In contrast to the fully connected case, with Drake Passage closed, the Atlantic circulation changes monotonically (but discontinuously) to a single-cell, northern-sinking state without the southern to northern-sinking bifurcation seen in Figure 6. However, the same bifurcation occurs on the return branch instead of the outward branch, with a dramatic switch from a single positive Atlantic cell to a single negative Atlantic cell, in a form of “overshoot”, coupled to a decrease in the Pacific positive cell and an increase in the Pacific negative cell.

4.5 The effect of wind forcing and a barotropic ACC

With such a simplified ocean model, and without any form of atmosphere, it is appropriate to consider only very simple forms of wind forcing. Nevertheless, we can address two pertinent questions regarding the qualitative response of the model: the effect of a barotropic (depth-averaged) component to the model ACC driven by circumpolar winds in the southern ocean; and the effect of wind-driven gyres in the main basins.

Figure 10 shows the results of an experiment in which a barotropic ACC is created by introducing a zonally constant zonal wind stress at the southernmost grid point of amplitude 0.8 N m^{-2} giving a dimensional ACC transport of about 62 Sv. Comparison with Figure 6 shows that this causes the bifurcation to dominantly positive cells on the increasing- R branch to occur for smaller R . Meanwhile the region of Atlantic hysteresis is diminished, as the collapse of strong, positive overturning in the Pacific leads to a complete collapse of the

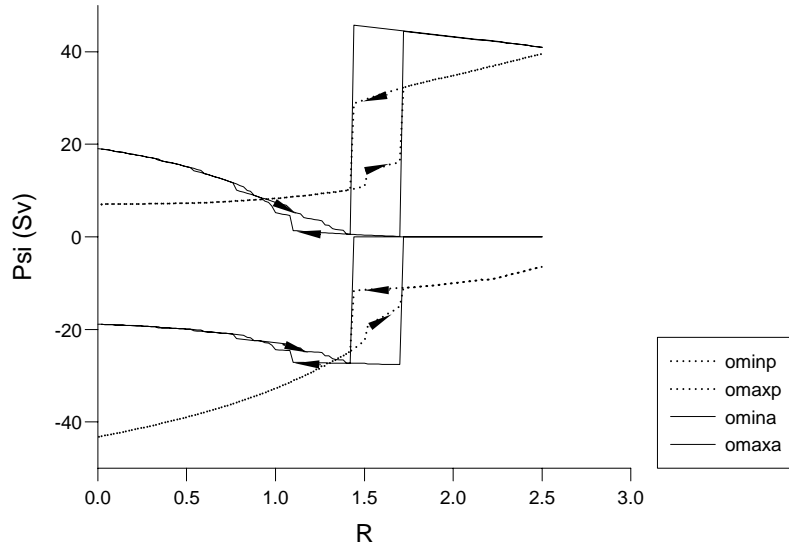


Figure 10: Maximum (positive) and minimum (negative) value of meridional overturning in the Atlantic, continuous line; and Pacific, dotted, for a sequence of runs with increasing and then decreasing relative salinity forcing amplitude R with a barotropic ACC transport of 62 Sv.

positive Atlantic cell on the return branch. Thus the addition of a barotropic ACC appears to lead to a stronger preference for similar circulation states in the two basins.

Figure 11 shows the effect of forcing the model with a zonal wind stress

$$\tau = \tau_0 \cos(2\pi\theta/\theta_1), \quad (4)$$

where θ is latitude. This gives a classical two-gyre pattern in the north and south Atlantic and south Pacific, and a single gyre in the north Pacific, as shown in figure 12. The amplitude τ_0 is set to 0.5 N m^{-2} , giving a maximum value for the barotropic streamfunction in the sub-tropical north Atlantic of 29 Sv.

The Pacific overturning curves are relatively little affected by this gyre-type wind pattern. In the Atlantic the effects are more pronounced. The positive overturning cell almost doubles in strength at $R = 1.2$ and the flow progresses

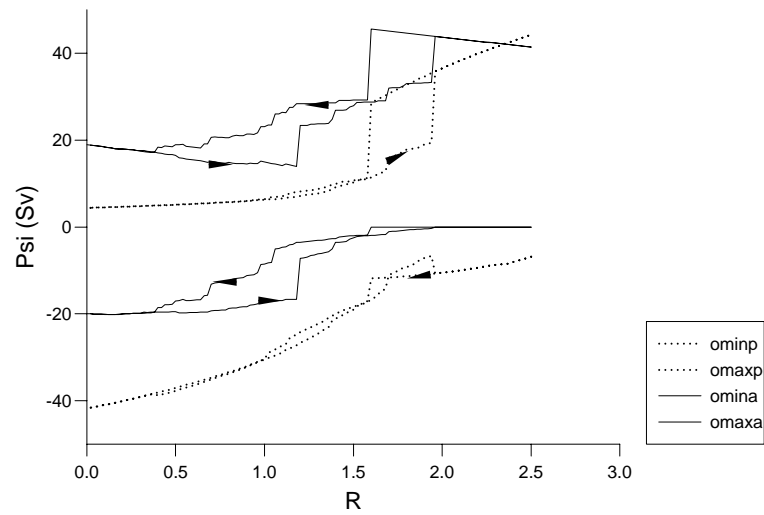


Figure 11: Maximum (positive) and minimum (negative) value of meridional overturning in the Atlantic, continuous line; and Pacific, dotted, for a sequence of runs with increasing and then decreasing relative salinity forcing amplitude R with the wind stress given by Eq. (4) with $\tau_0 = 0.5$ N.

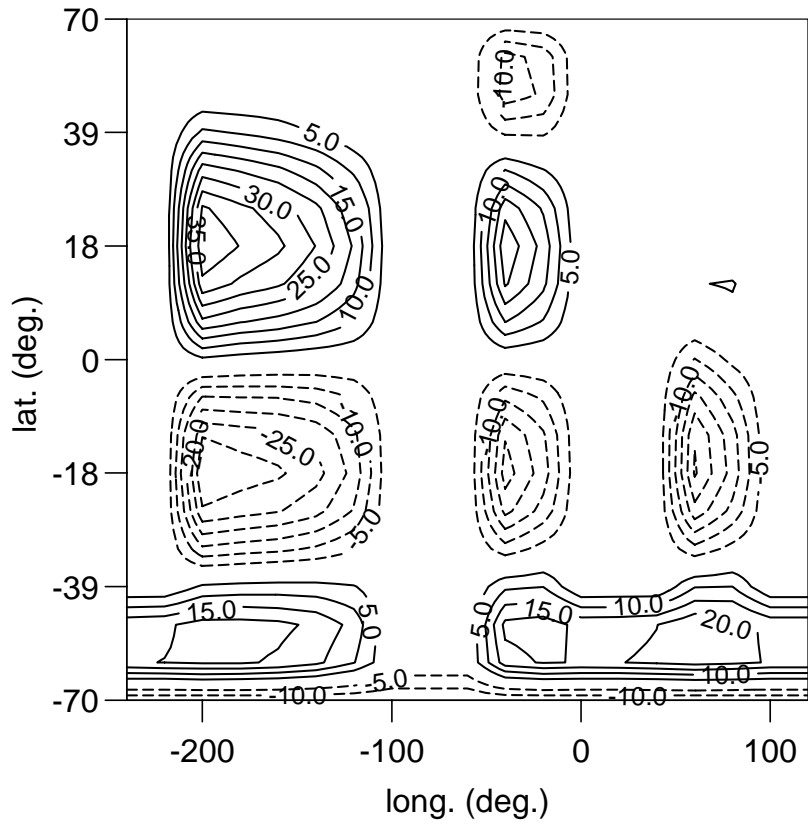


Figure 12: Barotropic streamfunction in Sv with the wind stress given by Eq. (4) with $\tau_0 = 0.5$ N.

to the single, positive cell state, without passing through a single, negative cell state. The maximum overturning achieved in the Atlantic is 6% greater than in case C without wind. Similar results are obtained if τ_0 is doubled. The effect of wind on meridional overturning has been examined in more detail by Zhang et al. (1992) and by EWK. Typically wind forcing in the subtropical gyre deepens the thermocline there and thus enhances meridional overturning.

4.6 Effects of bottom topography

We now consider briefly the possible effect on the behaviour seen above of allowing for non-trivial bottom topography. We consider two simple classes of topographic feature. In the first case we add mid-ocean ridges in the Indian and Atlantic oceans, and in the second a rise to the north in the north Atlantic. The mid-ocean ridges extend from southern to the northern boundary in both oceans and are one grid cell wide and one grid cell high, corresponding to a ridge height of about 1.1 km, except in the Southern Ocean south of the Indian where the ridge is raised to 2 gridpoints, around 2 km, to represent the Kerguelen plateau. The north Atlantic rise is modelled as a series of three, one grid-cell steps in the three northernmost Atlantic points. This corresponds to a zonally uniform rise from a depth of 4 km at around 40°N to a depth of 1400 m at 70°N . Plots of the extremal values of meridional overturning for these two sequences are shown in figures 13 and 14. Both are similar to the standard, flat bottom case C seen in Figure 6, except that the northern-sinking Atlantic state is destabilized on the return branch which bifurcates directly to a southern-state for $R \approx 1.5$ in both cases, recalling somewhat the “overshoot” which occurs on the return branch in case D, figure 9. In the mid-ocean ridge case the northern-sinking solution recovers fully at $R \approx 1.4$ but in the north Atlantic rise case there is no such recovery and dominantly northern sinking states are not found below $R \approx 1.5$. Thus the north Atlantic rise appears to destabilize northern sinking, as found by EWK. Note that the barotropic component to the ACC induced by the topography in these runs is typically very small. Almost identical behaviour was found when the sequences were repeated with the induced barotropic ACC artificially set to zero.

4.7 Effects of resolution

In ES it was shown that, in a single basin, the present model easily generalises to a hierarchy of models of varying resolution. Constructing and analysing an entire hierarchy of global models would be a major undertaking, but a relatively simple test is to repeat one of the above bifurcation sequences at twice the standard resolution. To reduce the computational costs we increase horizontal and vertical resolution separately. This has the added advantage of separating their relative influences on the solution.

The results of repeating the bifurcation sequence for the fully connected, flat bottom domain without wind, case C, at twice the horizontal resolution

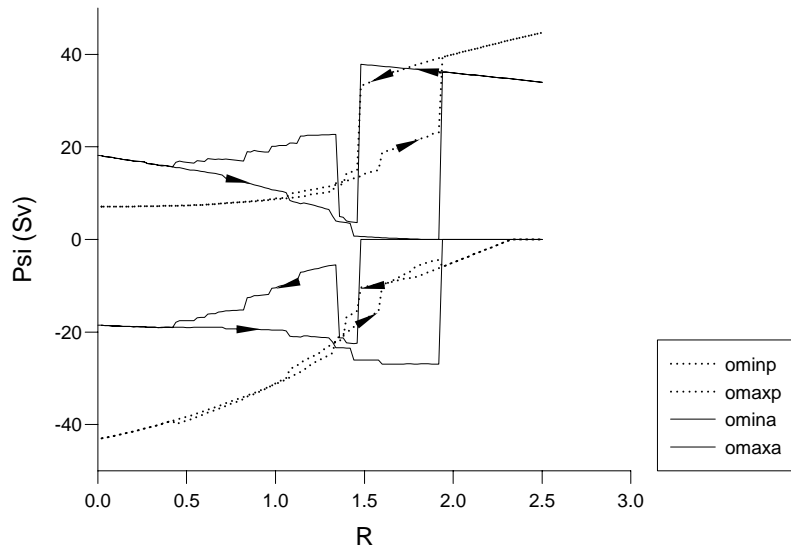


Figure 13: Maximum (positive) and minimum (negative) value of meridional overturning in the Atlantic, continuous line; and Pacific, dotted, for a sequence of runs with increasing and then decreasing relative salinity forcing amplitude R with mid-ocean ridges.

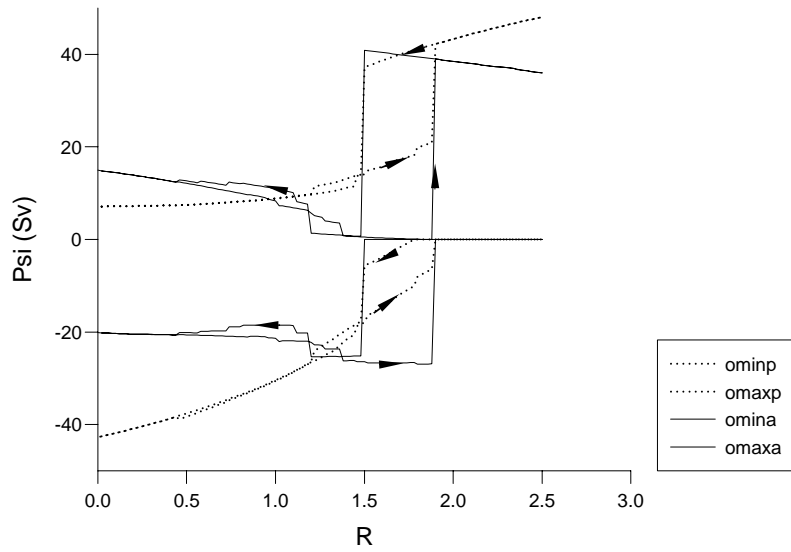


Figure 14: Maximum (positive) and minimum (negative) value of meridional overturning in the Atlantic, continuous line; and Pacific, dotted, for a sequence of runs with increasing and then decreasing relative salinity forcing amplitude R with a shallowing to the north in the north Atlantic.

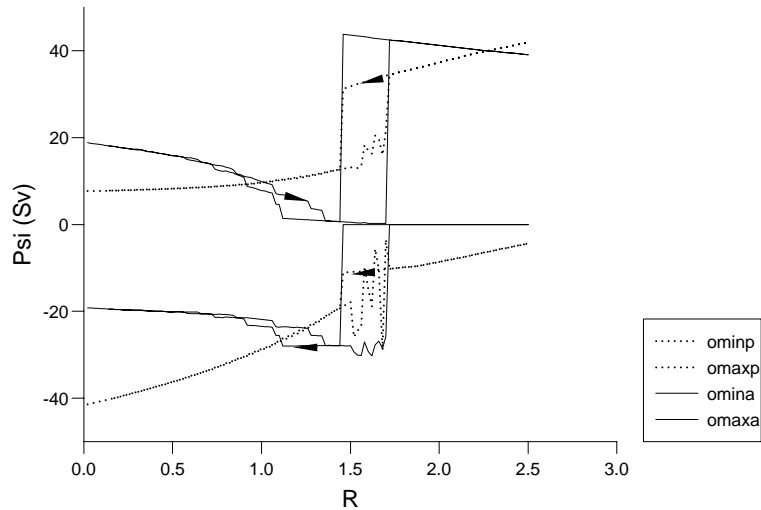


Figure 15: Maximum (positive) and minimum (negative) value of meridional overturning in the Atlantic, continuous line; and Pacific, dotted, for a sequence of runs with increasing and then decreasing relative salinity forcing amplitude R in the fully connected model, case C, at twice the horizontal resolution.

are shown in figure 15. In many respects the figure resembles qualitatively, and indeed quantitatively, the corresponding figure, 6, derived at low resolution. On the other hand, in common with the simulations with a barotropic ACC and with a rise in the north Atlantic, the extended region of Atlantic hysteresis for $R < 1.5$ does not occur. Once again, the model appears to prefer similar circulation states in the two main basins. More striking is the appearance of a region of variability close to the main bifurcation on the increasing- R branch. This is a region of regular oscillations which is not easily accessible; various single runs with simple initial conditions all converged to steady states. The oscillations have a period of around 200 years, and are characterised by a relatively short phase of enhanced deep convection and deep sinking at the southern boundary of the Pacific, followed by a longer phase in which the resulting deep salinity anomaly in the south Pacific decays, while deep salinity in the north Pacific increases. A detailed analysis of the oscillations is outside

the scope of this work but we intend to discuss oscillatory modes of the model in a forthcoming paper in which an atmospheric EBM is added to the system.

By contrast, doubling the vertical resolution has relatively little effect, with only minor differences to the behaviour evident in the corresponding bifurcation sequence (not shown).

5 Discussion

Simple, 3-D ocean models have several major advantages over 2-D models for climate studies. Firstly the ability to model geometric and topographic effects on the circulation directly, for instance the difference between deep sinking in the Labrador and GIN seas, which may be a crucial element of the Dansgaard-Oeschger cycle (Stocker 2000). Scalability is a second major advantage; the effects of low resolution in the third dimension can readily be determined by increasing the resolution, whereas the effects of removing the third dimension entirely are not so straightforward to determine. Third, and perhaps most important, 2-D models are incapable of directly representing the dominant (geostrophic) momentum balance in large-scale flows which relates the northward velocity to the eastward pressure gradient. In the 2-D model of Wright and Stocker (1991) the northward velocity is related instead to the northward pressure gradient by a constant which depends on latitude but not on the density structure. In a geostrophic flow the primary response to the northward pressure gradient is an eastward flow, thus a zonal overturning. Northward flow, hence meridional overturning, occurs only as a secondary response, driven by the action of the zonal overturning on the isopycnal surfaces. The relation between northward flow and pressure gradient thus has a complicated dependence on the density structure. Parameterizations of this dependence based on current climatic conditions may well be invalid for periods with significantly different ocean circulation. Another advantage of 3-D models is that they can represent the horizontal gyre circulations directly. As noted in the Introduction and in Section 3, at our standard, 18×18 resolution, horizontal gyre circulations must be viewed as being represented, rather than resolved, much in the way that the meridional overturning cells of the thermohaline circulation are represented by box models. Similarly, 0.25 degree-resolution OGCM runs have sometimes been described as eddy-permitting, rather than eddy-resolving. Our standard resolution thus represents an interesting hybrid between box models and resolved models, and is close to the minimum resolution for a 3-D global domain. However, even with only three boxes across the basin, there is clearly visible east-west asymmetry in the wind-driven gyre circulation in the Atlantic shown in figure 12. As described by EWK wind driving leads directly to meridional overturning and also distorts the isopycnal surfaces, thus leading to an indirectly wind-forced overturning that tends to counteract the direct forcing. Density variations over topography also produce barotropic and hence meridional overturning flow. In our 3-D model, all these

effects can, at least, be represented. In 2-D models they must somehow be parameterized.

As shown by Hines and Killworth (2001), and in common with most coarse-resolution ocean models, the present model suffers from unrealistically warm deep water and weak vertical temperature gradients, even at 2-degree resolution. However, at present we are interested in its qualitative behaviour under a wide range of forcing conditions. Detailed, quantitative validation of such a simple model against data restricted to present conditions seems to us inappropriate at this stage. Our immediate priority is to improve model dynamics and property transport by implementing an isopycnal diffusion scheme.

On the other hand, the bifurcation sequences obtained here are sufficiently intriguing that further investigation with more realistic models would certainly be worthwhile, if potentially costly. In particular, there is a strong preference in the model for similar circulation states in the Atlantic and Pacific, hence the present situation in the real ocean, with no deep sinking in the north Pacific, does not appear to be a robust state in our model. Whether this is simply a result of the coarse resolution, or our choice of initial conditions, deserves further investigation. The “averaging” of behaviour between the model Atlantic and Pacific must be communicated by a mixing of density through the southern ocean. In accordance with this interpretation an even greater preference for similar circulation states was obtained with the addition of a barotropic ACC. Pole-to-pole circulation modes can be considered to be driven by, typically very small, differences in surface density between the polar regions (Marotzke and Klinger 2000) thus the behaviour observed could be caused by relatively weak transport of density through the southern ocean. With our boundary conditions there must be a net flux of salinity out of the Pacific and Indian oceans and into the Atlantic at steady state. Examination of steady, northern-sinking, states at $R = 1.75$ and $R = 2$ shows that there is indeed a net flux of salinity into the Atlantic (of magnitude corresponding to about 0.1 Sv fresh water) but the net density flux must be out of the Atlantic, since there is a compensatory temperature flux import around 30 times larger. This density flux is thus of the correct sign to promote the northern sinking state in the Atlantic, presumably at the cost of the strength of northern sinking in the Pacific, as observed in the bifurcation sequences. For the solution found in Section 3 at $R = 1$, in which both Atlantic and Pacific have a dominantly southern-sinking circulation, we find a density flux of similar order, this time into the Atlantic, and thus again of the correct sign to strengthen the Atlantic overturning.

Single runs at constant salinity forcing have shown that for values of R above 2.5, the Atlantic circulation in the fully connected domain can collapse to a state intermediate between the thermally forced, polar-sinking states found so far, and salinity driven, equatorially sinking states. In the fully collapsed Atlantic state a shallow, upper layer circulation is dominated by saline forcing, with weak sinking near the equator and upwelling at the poles. Previous experience with the same model in a single basin suggests such circulations

are liable to feature oscillatory, flush-collapse cycles (EWK) but in the present model, for the values of R tested, no thermal flush occurred in the first 8000 years in these runs although the deep temperature increased throughout. Oscillatory modes have, however, been found at doubled resolution, figure 15, and also in a version coupled to a simple, energy-balance atmosphere. These results will be discussed in a subsequent article.

6 Conclusions

In relation to our first principal objective, of testing the feasibility of long-term, global, 3-D simulations, the results obtained above indicate that such simulations are certainly possible at low resolution. For our coarsest (18×18) latitude/longitude grid, we can undertake a million-year integration on a single node of an SGI Origin 2000 machine overnight. Each of the bifurcation diagrams we have plotted (Figures 7 to 12) represents 1 million years of model integration time and around 14 to 16 hours cpu. Allowing for modest parallelisation or other enhancement in either hardware or numerics, such as implicit time-stepping, it would therefore be feasible to undertake calculations for several hundred thousand model years overnight even at substantially higher resolution (and thus also with more realistic topography).

In relation to our second objective, of investigating the stable states of our simplified global model, we have found that the stability and bifurcation behaviour of the oceanic THC is sensitive to inter-basin geometry and connectivity, as well as to certain types of topographic variation and wind forcing. In particular, the model Pacific circulation was found to be strongly influenced by the presence of the Atlantic, even with Drake Passage closed. This sensitivity means, *inter alia*, that results from strictly 2-D models cannot be regarded as more than illustrative, although it is possible that multi-basin 2-D representations may, with appropriate parameterisation, still yield qualitatively similar behaviour to 3-D representations. With such a coarse resolution and deliberately over-simplified model as that used here we cannot regard our 3-D results as much more than illustrative either. They demonstrate clearly, however, that extensive exploration of the behaviour of suitable, non-eddy-resolving 3-D models, with appropriate physics for long-term, large-scale processes is now possible. With less idealised representations at moderate resolution, detailed comparison with the results of higher resolution 3-D OGCM's will be possible.

Acknowledgements

We wish to acknowledge the financial support of the UK NERC, as well as helpful comments and suggestions from A. Ganopolski, P.D. Killworth, J. Marotzke and A.J. Willmott.

Appendix. Treatment of islands and straits

Vertical integration of the momentum equations leads to an elliptic equation for the barotropic streamfunction, Ψ , which defines the depth-averaged flow \mathbf{u}^+ where

$$H\mathbf{u}^+ = \int_{-H}^0 \mathbf{u} dz = \mathbf{k} \times \nabla \Psi, \quad (5)$$

where H is the ocean depth and the surface is at $z = 0$. \mathbf{k} is a unit vector in the vertical. The equation for Ψ is given by EWK. The streamfunction Ψ must take a constant value on the domain boundaries to satisfy the condition of zero normal flow but the boundary value can be different on each isolated landmass (or island). In our standard geometry we can take the boundary value on the northern landmass to be zero, without loss of generality, then the value of Ψ on the coast of Antarctica, which is the only other island in our standard geometry, determines the barotropic flow around Antarctica. It is important to realize (McWilliams 1977) that the value of Ψ on islands cannot be freely specified since the following constraint, arising from the integration of the depth-averaged momentum equations around the island, must be satisfied:

$$\oint \left(\lambda \mathbf{u}^+ - \frac{\boldsymbol{\tau}_0}{H} \right) \cdot d\mathbf{l} = 0 \quad (6)$$

where λ is the drag coefficient and $\boldsymbol{\tau}_0$ the wind stress and the integral is taken around the island boundary. This constraint can be satisfied very simply in the time-independent, linear momentum balance of the frictional geostrophic system. We first decompose the streamfunction into two parts, Ψ_I and Ψ_B , the first resulting from the interior wind and topographic forcing with a value of zero on all coasts, and the second from the, as yet unknown, boundary condition on the island, with zero interior forcing. Thus their sum $\Psi = \Psi_I + \Psi_B$, can satisfy the governing equation in the interior and the boundary condition. The function Ψ_B is determined by solving the interior equation with zero forcing and unit boundary condition on the island, then multiplying the solution by a constant in order that the complete streamfunction Ψ satisfies the constraint (6). The value of the constant is then the boundary value of Ψ on the island. For a system of n islands the procedure easily generalises to a system of $n - 1$ linear equations for the coefficients of $n - 1$ boundary streamfunctions.

We solve the elliptic equation for the barotropic streamfunction by Gaussian elimination. Adjacent to boundaries we use a second order, one-sided difference to calculate the normal density gradient required for the baroclinic tangential velocity calculation. In straits and channels one or two points wide the cross-channel (geostrophic) pressure gradient is assumed to be zero and the flow is therefore driven purely by the along-channel pressure gradient and friction. The velocity under-relaxation parameter δ defined by ES is set to 0.8.

REFERENCES

- Bryan F (1986) High-latitude salinity effects and interhemispheric thermohaline circulations. *Nature* 323: 301–304
- Dijkstra HA, Neelin JD (2000) Imperfections of the thermohaline circulation: latitudinal asymmetry and preferred northern sinking. *J Clim* 13: 366–382
- Edwards NR, Willmott AJ, Killworth PD (1998) On the role of topography and wind stress on the stability of the thermohaline circulation. *J Phys Oceanog* 28: 756–778
- Edwards NR, Shepherd JG (2001) Multiple thermohaline states due to variable diffusivity in a hierarchy of simple models. *Ocean Modelling* 3: 67–94
- Hines A, Killworth PD (2001) An inversion-assimilation approach using hydrographic data in a coarse resolution ocean model. *J Atmos Oceanic Tech*: in press
- Lenderink G, Haarsma RJ (1994) Variability and multiple equilibria of the thermohaline circulation, associated with deep water formation. *J Phys Oceanog* 24: 1480–1493
- McWilliams JC (1977) *Dyn Atm Oceans* 1: 427–441
- Manabe S, Stouffer RJ (1988) Two stable equilibria of a coupled ocean-atmosphere model. *J Clim* 1: 841–866
- Marotzke J, Klinger BA (2000) The dynamics of equatorially asymmetric thermohaline circulations. *J Phys Oceanog* 30: 955–970
- Marotzke J, Welander P, Willebrand J (1988) Instability and multiple steady states in a meridional-plane model of thermohaline circulation. *Tellus* 40A: 162–172
- Marotzke J, Willebrand J (1991) Multiple equilibria of the global thermohaline circulation. *J Phys Oceanog* 21: 1372–1385
- Rahmstorf S (1994) Rapid climate transitions in a coupled ocean-atmosphere model. *Nature* 372: 82–85
- Rahmstorf S (1995) Bifurcations of the Atlantic thermohaline circulation in response to changes in the hydrological cycle. *Nature* 378: 145–149
- Samelson RM, Vallis GK (1997) A simple friction and diffusion scheme for planetary geostrophic basin models. *J Phys Oceanog* 27: 186–194
- Stocker TF (2000) Past and future reorganizations in the climate system. *Quaternary Science Reviews* 19: 301–319

- Stocker TF, Wright DG (1991) Rapid transitions of the ocean's deep circulation induced by changes in surface water fluxes. *Nature* 351: 729–732
- Thual O, McWilliams JC (1992) The catastrophe structure of thermohaline convection in a two-dimensional fluid model and a comparison with low-order box models. *Geophys Astrophys Fluid Dynamics* 64: 67–95
- Winton M, Sarachik E (1993) Thermohaline oscillations induced by strong steady salinity forcing of ocean general circulation models. *J Phys Oceanog* 23: 1389–1410
- Wright DG, Stocker TF (1991) A zonally averaged ocean model for the thermohaline circulation. 1. Model development and flow dynamics. *J Phys Oceanog* 21: 1713–1724
- Zhang SC, Lin A, Greatbach RJ (1992) A thermocline model for ocean-climate studies. *J Mar Res* 50: 99–124